

Reaction-diffusion model for the growth of avascular tumor

S. C. Ferreira, Jr.,^{1,*} M. L. Martins,^{2,†} and M. J. Vilela³

¹*Departamento de Física, Instituto de Ciências Exatas, Universidade Federal de Minas Gerais, Caixa Postal 702, 30161-970 Belo Horizonte, Minas Gerais, Brazil*

²*Departamento de Física, Universidade Federal de Viçosa, 36571-000 Viçosa, Minas Gerais, Brazil*

³*Departamento de Biologia Animal, Universidade Federal de Viçosa, 36571-000 Viçosa, Minas Gerais, Brazil*

(Received 25 September 2001; revised manuscript received 26 October 2001; published 23 January 2002)

A nutrient-limited model for avascular cancer growth including cell proliferation, motility, and death is presented. The model qualitatively reproduces commonly observed morphologies for primary tumors, and the simulated patterns are characterized by its gyration radius, total number of cancer cells, and number of cells on tumor periphery. These very distinct morphological patterns follow Gompertz growth curves, but exhibit different scaling laws for their surfaces. Also, the simulated tumors incorporate a spatial structure composed of a central necrotic core, an inner rim of quiescent cells and a narrow outer shell of proliferating cells in agreement with biological data. Finally, our results indicate that the competition for nutrients among normal and cancer cells may be a determining factor in generating papillary tumor morphology.

DOI: 10.1103/PhysRevE.65.021907

PACS number(s): 87.10.+e, 87.18.Hf, 87.15.Vv

I. INTRODUCTION

Cancer is a disease derived, with few exceptions, from mutations on single somatic cells that disregard the normal controls of proliferation, invade adjacent normal tissues, and give rise to secondary tumors (metastasis) on sites different from its primary origin [1]. Although cancers are extremely diverse and heterogeneous, a small number of pivotal steps associated with both deregulated cell proliferation and suppressed cell death is required for the development of any and all tumors. Indeed, all neoplasms evolve according to a universal scheme of progression [2,3]. Neoplastic cells accumulate a series of genetic or epigenetic changes along the tumor progression in response to natural selection and as an integrated defense program against stress situations similar to the response of a bacterial colony facing severe and sustained threats [4]. But, unlike bacterial growth, tumor progression involves a complex network of interactions among cancer cells and its host microenvironment [5]. It is well known that stressed bacterial colonies can develop diffusion-limited fractal patterns [6,7]. Recently, normal and tumor cell patterns *in vivo* and *in vitro* were characterized by their fractal dimensions and cluster size distribution functions [8–10], reinforcing the great current interest in the search for basic principles of growth in living organisms, which are the most complex and challenging self-organized systems. In particular, for cancer growth, one of the most aggressive phenomena in biology, numerous mathematical models have recently been investigated. Examples include studies, based on classical reaction-diffusion equations, of the growth of tumor spheroids [11], cancer evolution and its interaction with the immune system [12], and the fundamental problem of tumor angiogenesis [13,14].

Recently, we [15,16] proposed a diffusion-limited model to simulate the growth of carcinoma *in situ* in which cell

proliferation, motility, and death are locally regulated by the concentration of growth factors produced by each cancer cell. This model was able to generate compact, connected, and disconnected morphologies that progress in time according to Gompertz growth curves, and for which the tumor gyration radii scale as in the Eden model for an asymptotically large number of cells. These features were shown to be independent of the detailed functional form of the microscopic growth rules. In contrast, the structure of the tumor border is influenced by the nature of the growth rules as indicated by the different scaling laws for the number of peripheral cancer cells. In particular, for disconnected and connected patterns the surface widths scale with exponents similar to those observed in bacterial colonies. Although the similarities between the simulated and histological tumor patterns were encouraging, the model was unable to generate papillary and ramified morphologies found in many of epithelial cancers and trichoblastomas. In consequence, we were led to investigate the role of nutrient competition in neoplastic development, a biological feature excluded in our previous model but central in the growth of fractal bacterial colonies. Indeed, cancer cells subvert the evolutionary adaptations to multicellularity and revert to a largely nutrient-limited style of growth.

In this paper we analyze the avascular cancer growth in a model including cell proliferation, motility, and death as well as competition for nutrients among normal and cancer cells. The cell actions (division, migration, and death) are locally controlled by the nutrient concentration field. In Sec. II we introduce the cancer growth model. In Sec. III the simulation results for the tumor patterns, growth curves, and scaling laws are discussed. In Sec. IV the diffusion of growth factors secreted by the cancer cells are added to the nutrient-limited model. Finally, we draw some conclusions in Sec. V.

II. THE CANCER GROWTH MODEL

The basic biological principles included in the model are cell proliferation, motility, and death, and competition for

*Electronic address: silviojr@fisica.ufmg.br

†Electronic address: mmartins@mail.ufv.br

nutrients among normal and cancer cells. Nutrients (oxygen, amino acids, glucose, metal ions, etc.) diffuse from a capillary vessel through the tissue towards the individual (normal and cancer) cells. Under restricted nutrient supply the growth rate of cancer cells is limited by its ability to compete for nutrients with the normal cells. In our model the division, migration, and death of each cancer cell is controlled by the nutrient concentration in its local microenvironment.

A. The tissue

The studied system consists of a tissue fed by a single capillary vessel. The tissue is represented by a square lattice of size $(L+1) \times (L+1)$ and lattice constant Δ . The capillary vessel, localized at the top of the lattice at $x=0$, is the unique source from which nutrients diffuse through the tissue towards the individuals cells. Although a tumor mass is composed of different cell subpopulations [2], we shall consider only three types: normal, cancer, and tumor necrotic cells. Any site, with coordinates $\vec{x}=(i\Delta, j\Delta)$, $i, j=0, 1, 2, \dots, L$, is occupied by only one of these cell types. In contrast to normal cells, one or more cancer cells can pile up in a given site. In turn, tumor necrotic cells are inert and, for simplicity, will be considered always as a single dead cell. Thus, each lattice site can be thought of as a group of actual cells in which the normal, necrotic, and cancer cell populations assume one of the possible values $\sigma_n(\vec{x}, t) = \sigma_d(\vec{x}, t) = 0, 1$ and $\sigma_c(\vec{x}, t) = 0, 1, 2, \dots$, respectively. As initial ‘‘seed’’ a single cancer cell in the half of the lattice ($x=L\Delta/2$) and at a distance Y from the capillary vessel is introduced in the normal tissue, in agreement with the theory of the clonal origin of cancer [17]. Periodic boundary conditions along the horizontal axis are used. The row $i=0$ represents a capillary vessel and the sites with $i=L+1$ constitute the external border of the tissue.

B. The nutrients

As considered by Scalerandi *et al.* [18], we assume that dividing cancer cells are especially vulnerable to some critical nutrients such as iron, essential for DNA synthesis and, therefore, for cell division. The many other nutrients necessary for eucariotic cells are supposed to affect mainly the motility and death of the cancer cells. So, the nutrients are divided into two groups: essential and nonessential for cell proliferation, described by the concentration fields $N(\vec{x}, t)$ and $M(\vec{x}, t)$, respectively. However, it is assumed that both nutrient types have the same diffusion coefficients and consumption rates by the normal cells. These concentration fields obey the diffusion equations

$$\begin{aligned} \frac{\partial N(\vec{x}, t)}{\partial t} = & D\nabla^2 N(\vec{x}, t) - \gamma N(\vec{x}, t) \sigma_n(\vec{x}, t) \\ & - \lambda_N \gamma N(\vec{x}, t) \sigma_c(\vec{x}, t) \end{aligned} \quad (1)$$

and

$$\begin{aligned} \frac{\partial M(\vec{x}, t)}{\partial t} = & D\nabla^2 M(\vec{x}, t) - \gamma M(\vec{x}, t) \sigma_n(\vec{x}, t) \\ & - \lambda_M \gamma M(\vec{x}, t) \sigma_c(\vec{x}, t) \end{aligned} \quad (2)$$

in which the nutrient absorption terms are proportional to the cell populations present in each site, and it is assumed differentiated nutrient consumption rates for normal and cancer cells by factors λ_N and λ_M . It is important to notice that the present model assumes the simplest form for the nutrient diffusion phenomena, i.e., linear equations with constant coefficients. Also, $\lambda_N > \lambda_M$ is used, reflecting the larger cancer cells affinity for essential nutrients.

The boundary conditions satisfied by the nutrient concentration fields are $N(x=0) = M(x=0) = K_0$, representing the continuous and fixed supplies of nutrients provided by the capillary vessel; $N(y=0) = N(y=L\Delta)$ and $M(y=0) = M(y=L\Delta)$, corresponding to the periodic boundary conditions along the x axis; finally, Neumann boundary conditions, $\partial N(x=L\Delta)/\partial y = \partial M(x=L\Delta)/\partial y = 0$, are imposed on the border of the tissue. The hypothesis that a blood vessel provides a fixed nutrient supply to the cells in a tissue is a simplification that neglects the complex response of the vascular system to metabolic changes of cell behavior [19].

In order to reduce the number of parameters in Eqs. (1) and (2), the new dimensionless variables are defined,

$$\begin{aligned} t' = \frac{Dt}{\Delta^2}, \quad \vec{x}' = \frac{\vec{x}}{\Delta}, \quad N' = \frac{N}{K_0}, \\ M' = \frac{M}{K_0}, \quad \alpha = \Delta \sqrt{\frac{\gamma}{D}}. \end{aligned} \quad (3)$$

Using these new variables in Eqs. (1) and (2) and omitting the primes, we obtain

$$\frac{\partial N}{\partial t} = \nabla^2 N - \alpha^2 N \sigma_n - \lambda_N \alpha^2 N \sigma_c \quad (4)$$

and

$$\frac{\partial M}{\partial t} = \nabla^2 M - \alpha^2 M \sigma_n - \lambda_M \alpha^2 M \sigma_c \quad (5)$$

for the diffusion equations describing the nutrients concentration fields. In addition, the boundary condition on the capillary vessel becomes $N(x=0) = M(x=0) = 1$ and a value $\Delta = 1$ is defined.

C. Cell dynamics

Each tumor cell can be selected at random, with equal probability, and carry out one of three actions.

(1) *Division*. Cancer cells divide by mitosis with probability P_{div} . If the chosen cell is inside the tumor, its daughter will pile up at that site, and $\sigma_c(\vec{x}) \rightarrow \sigma_c(\vec{x}) + 1$. Otherwise, if the selected cell is on the tumor border, its daughter cell will occupy at random one of their nearest neighbor sites \vec{x}' containing a normal or a necrotic cell and, therefore, $\sigma_c(\vec{x}') = 1$ and $\sigma_{n,d}(\vec{x}') = 0$. The mitotic probability P_{div} is deter-

mined by the concentration per cancer cell of the essential nutrients N present on the microenvironment of the selected cell,

$$P_{\text{div}}(\vec{x}) = 1 - \exp\left[-\left(\frac{N}{\sigma_c \theta_{\text{div}}}\right)^2\right]. \quad (6)$$

The Gaussian term is included in order to produce a sigmoid curve saturated to the unity, and the model parameter θ_{div} controls the shape of this sigmoid.

(2) *Migration.* Cancer cells migrate with probability P_{mov} . A selected cell inside the tumor, at a site \vec{x}_i , will move to a nearest neighbor site \vec{x}' chosen at random. Thus, $\sigma_c(\vec{x}') \rightarrow \sigma_c(\vec{x}') + 1$ and, clearly, $\sigma_c(\vec{x}) \rightarrow \sigma_c(\vec{x}) - 1$. Otherwise, if the selected cell is on the tumor border, the invasion of a normal or necrotic nearest neighbor site will be dependent on the number of cancer cells present in the selected site. If in this site there is a single cancer cell, it migrates by interchanging its position with that of the invaded one. If there are other cancer cells in the same site of the one selected to move, the migrating cell will occupy the position of the normal or necrotic nearest neighbor cell, which, in turn, disappears. In terms of cell populations the migration of a cell on the tumor border corresponds to the following operations: $\sigma_c(\vec{x}') = 1$, $\sigma_c(\vec{x}) \rightarrow \sigma_c(\vec{x}) - 1$, $\sigma_{n,d}(\vec{x}') = 0$, and $\sigma_{n,d}(\vec{x}) = 1$ if $\sigma_c(\vec{x}) = 1$. The probability of cell migration P_{mov} has the same functional form of P_{div} , but depends on the concentration of the nonessential nutrients M present on the microenvironment of the selected cell and increases with the local population of cancer cells. So,

$$P_{\text{mov}}(\vec{x}) = 1 - \exp\left[-\sigma_c \left(\frac{M}{\theta_{\text{mov}}}\right)^2\right] \quad (7)$$

with the model parameter θ_{mov} controlling the shape of this sigmoid.

(3) *Cell death.* Cancer cells die transforming into a necrotic cell with probability P_{del} . Thus, $\sigma_c(\vec{x}) \rightarrow \sigma_c(\vec{x}) - 1$ and $\sigma_d(\vec{x}) = 1$ when σ_c vanishes. The cell death probability P_{del} is determined by the concentration per cancer cells of the nonessential nutrients M present on the microenvironment of the selected cell,

$$P_{\text{del}}(\vec{x}) = \exp\left[-\left(\frac{M}{\sigma_c \theta_{\text{del}}}\right)^2\right], \quad (8)$$

a Gaussian distribution whose variance depends on the model parameter θ_{del} .

The cell dynamics rules used in our model take into account that, as the cancer growth progresses, cell migration increases near the border of the tumor due to the high availability of nutrients and the increase in the number of cancer cells, which release a series of enzymes (collagenases, metalloproteinases, etc.) responsible for the progressive destruction of the extracellular matrix. Also, in the regions where there is a high population density and an ineffective supply of nutrients via diffusion processes, the cell division is inhibited and, at the same time, the probability of cell death increases. But, under these rules cell growth and migration is

possible even inside the tumor. Finally, the model parameters θ_{div} , θ_{mov} , and θ_{del} , which characterize the cancer cells' response to nutrient concentrations and embody complex genetic and metabolic processes, should be interpreted in terms of the underlying biochemistry and molecular biology, a still open problem. The other three model parameters, α , λ_N , and λ_M , associated with the consumption of essential and non-essential nutrients for cell proliferation by the normal and cancer cells, should be more easily determined from biological experiments.

It is worthwhile to note that from the point of view of the so-called kinetic cellular theory, which provides a general framework for the statistical description of the population dynamics of interacting cells [12], the local probabilities P_{div} , P_{mov} , and P_{del} can be thought of as an effective kinetic cellular model.

D. Computer implementation

The growth model simulations were implemented using the following procedure. At each time step, the diffusion Eqs. (4) and (5) are numerically solved in the stationary state through relaxation methods, providing the nutrient concentration at any lattice site. Then, $N_C(t)$ cancer cells are sequentially selected at random with equal probability. For each one of them, a tentative action (division, death, or movement) is chosen at random with equal probability and the time is incremented by $\Delta t = 1/N_C(t)$. The selected cell action will be implemented or not according to the correspondent local probabilities determined by Eq. (6), (7), or (8). If the selected cell divides or dies, therefore, changing the number of cancer cells that consume nutrients, we solve the diffusion equations in a small neighborhood of linear size $l = 20$ centered in the altered site. This is done in order to take into account these local perturbations and to speed up the computer algorithm, since the number of numerical iterations needed to solve the diffusion equation is proportional to L^2 . At the end of this sequence of $N_C(t)$ tentatives, a new time step begins and the entire procedure (solution of the diffusion equations and application of the cell dynamics) is iterated. The simulations stop if any tumor cell reaches the capillary vessel. In all the simulations, the exact solutions for the stationary diffusion equations in the absence of tumor cells were used for the nutrient concentration fields at $t = 0$.

III. SIMULATIONAL RESULTS

In Fig. 1 the most commonly observed morphologies in tumor growth such as papillary, compact, and disconnected are shown. Disconnected patterns, typical of round cell neoplasias such as lymphoma, mastocytoma, and plasmacytoma, correspond to transient simulated patterns in which cancer cells have high motility but a low mitotic rate. In turn, if the cell migration is very small and the high mitotic rate demands large amounts of essential nutrients, then the simulated patterns exhibit fingerlike shapes similar to the papillary morphologies found in epithelial tumors, such as basal and skin cells carcinomas, and hepatomas. If nutrient availability in the tissue is further reduced by an increasing cell consumption, the papillarylike patterns become progres-

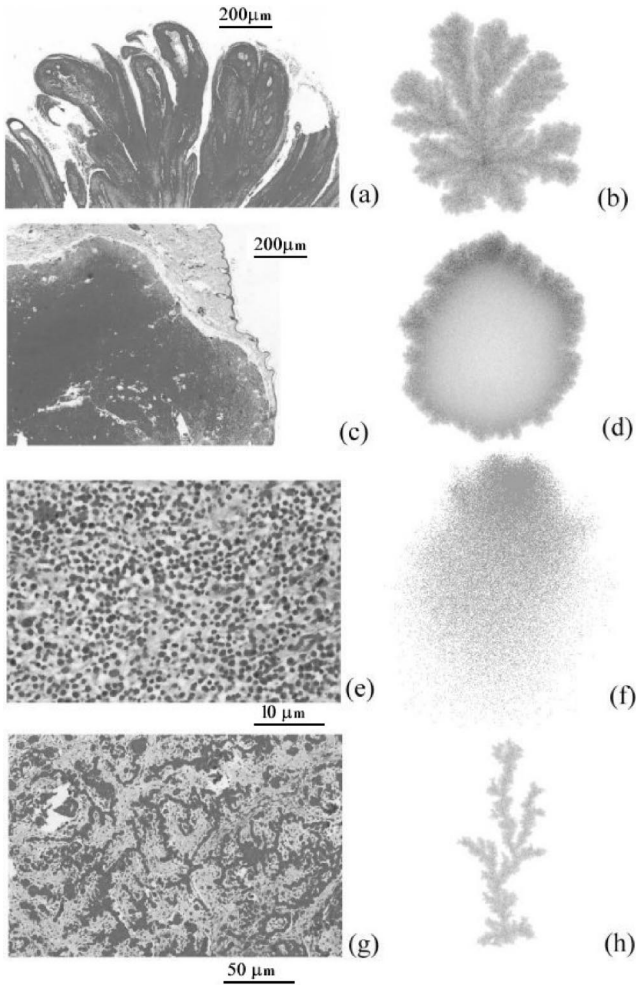


FIG. 1. Common morphologies observed in cancer growth. (a) Papillary pattern of a scamous papyloma, (c) a compact solid basocellular carcinoma, (e) a disconnected pattern of a plasmocytoma, and (g) characteristic cell filaments of a trichoblastoma. All these histological patterns were obtained from dogs. The corresponding simulated patterns are shown in (b), (d), (f), and (h), respectively.

sively thinner and similar to the chords or filaments of cells that constitute one of the hallmarks of the trichoblastoma morphology. Finally, under high nutrient supply, which means low cell consumption of both nutrient types, the simulated patterns are compact, such as those observed for solid tumors.

Typical patterns generated by the present model are shown in Figure 2. As one can see, nonspherical morphologies growing towards the capillary vessel are observed, according to the rigorous results for moving boundary problems of cancer growth [20]. The nutrient consumption by normal and cancer cells, controlled by the model parameters α , λ_N , and λ_M , plays a central role in morphology determination. For small values of these parameters, corresponding to growth conditions in which individual cells demand small nutrients supplies, the patterns tend to be compact and circular. However, if the mitotic rate of cancer cells is small due to the large amount of nutrients demanded for cell division, generating a significant nutrient competition, these compact patterns progressively assume papillarylike mor-

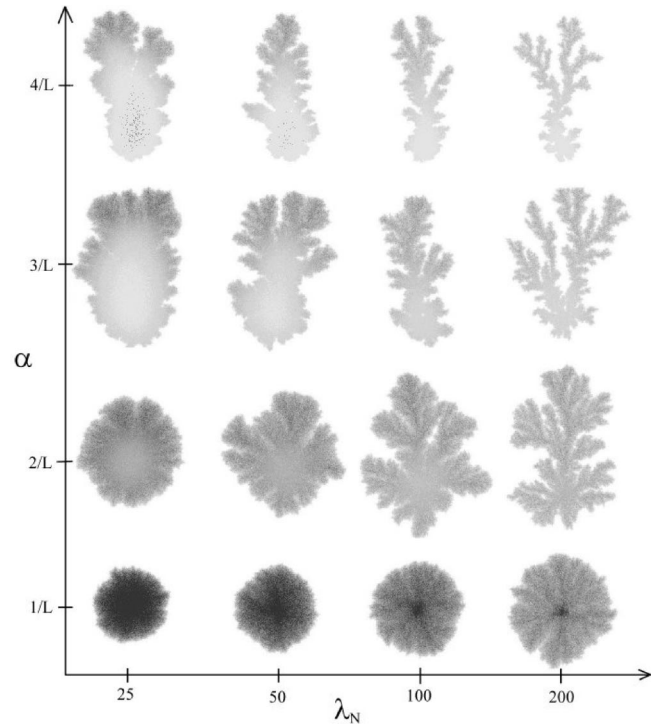


FIG. 2. Simulational results of the nutrient-limited cancer growth model. The patterns are organized as a function of nutrient consumption rate α for normal cells and the multiplicative factor λ_N to the consumption rate of mitotic essential nutrients by the cancer cells. The remaining four parameters of the model were fixed in $\lambda_M = 10$, $\theta_{div} = 0.3$, $\theta_{mov} = \infty$ (absence of cell migration) and $\theta_{del} = 0.01$. The patterns are drawn in a gray scale where the darker regions represent higher cancer cell populations. The tissue size is 500×500 , with the initial “cancer seed” 300 sites distant from the capillary. The total number of cancer cells depends on tumor morphology and attains up to 2×10^5 for compact patterns. The simulated patterns are compact for low λ_N values and become papillary or fingerlike for high λ_N . For the same λ_N the patterns are more papillary for higher α . Since the capillary vessel provides a fixed nutrient supply, the dimensionless consumption rate of the normal tissue α sets up the levels of available resources for which cancer cells compete. So, high α and/or λ_N values correspond to the limit of strong nutrient competition.

phologies. At high nutrient consumption rates these papillary patterns become the rule and, for low cancer cell division, continuously transform in thin tips, filaments, or chords of cells. Also, the smaller the α and λ_N values are, the larger the fraction of necrotic cancer cells for a fixed cellular response leading to cell death (controlled by θ_{del}) is. In particular, this fraction is smaller for papillary patterns than compact ones, suggesting that the optimal growth morphology under strong nutrients limitation is fractal. Finally, the higher cell migration is, the more homogeneous the patterns are, the faster the tumor growth is, and the smaller the fraction of necrotic cells is.

The tumor patterns generated by the present model were characterized by its gyration radius R_g , total number of cancer cells N_C , and number of cells on tumor periphery S (including the surface of holes, if any). The gyration radius R_g is defined as

TABLE I. Morphology, progress curves, and scaling laws for the patterns generated by the nutrient-limited model.

Morphology	Characteristic features	Growth in time			Exponents	
		N_C	R_g	S	ν	σ
Compact	Low nutrient consumption; Low cell motility	Gompertz	Gompertz	Gompertz	0.50	0.50
Papillary	High nutrient consumption; Low cell motility	Gompertz	Gompertz	Gompertz	0.50–0.60	0.60–1
Disconnected	Low mitotic rate; high cell motility; Transient behavior	Gompertz	Gompertz	Gompertz	0.50	1

$$R_g = \left(\frac{1}{n} \sum_{i=1}^n r_i^2 \right)^2, \quad (9)$$

where n is the number of sites occupied by the pattern (cancer or necrotic cells) and r_i is the distance of the occupied site i from the tumor mass center. These quantities could be related to clinically important criteria such as progress curves, rate of growth (volumetric doubling time) at given radii, proliferative and necrotic fractions of the tumor. In medicine, these data are used to determine a tumor's malignancy and its prognosis. The obtained results are summarized in Table 1.

Despite the detailed microscopic mechanisms of growth, for all the simulated patterns the progress in time of cancer cell populations follows a Gompertz curve,

$$N_C(t) = A \exp\{-\exp[-k(t-t_c)]\}, \quad (10)$$

as one can see in Fig. 3. Moreover, the tumor gyration radius R_g , as well as the number of peripheral cells S , also exhibits a Gompertz growth, contrary to the linear regimes observed for R_g and even S in our previous non-nutrient-limited model [16]. So, the present model reveals that the Gompertz law of growth for the cancer cell populations and tumor size is a robust emergent feature of cancer dynamics under nutrient competition. It is important to notice that linear or power law fittings for the growth in time of R_g and S can also be very satisfactory for several simulated patterns, therefore explaining our previous findings [16] and the recent experimental observations of brain tumors grown *in vitro* [21]. However, only the Gompertz law can provide good fittings for all the three quantities N_C , R_g , and S .

On the other hand, as a function of the total number of cancer cells, both R_g and S obey power law scaling given by $R_g \sim N_C^\nu$ and $S \sim N_C^\sigma$, respectively. For solid patterns these exponents are $\nu \sim 0.5$ and $\sigma \sim 0.5$, corresponding to effective circular and nonfractal patterns. As the nutrient consumption increases the patterns tend to papillarylike shapes for which the exponent σ increases towards the value 1 and the exponent ν varies in the range [0.50,0.60], indicating a fractal morphology for the tumor. It is important to mention that increasing cell motility contributes to round and homogenize

these patterns, progressively destroying their fractal features. Also, the tumor growth is faster for higher cancer cell migration.

An interesting result, shown in Fig. 4, is the existence of a necrotic core in the center of the simulated tumors for high nutrient consumption or cell division rates. As observed in real tumors and *in vitro* multicell spheroids [11], a simulated pattern consists of three distinct regions: a central necrotic core, an inner rim of quiescent cancer cells, and a narrow outer shell of proliferating cells. These different regions are evident in Fig. 5 where the cancer cell density and average cell division rate are plotted for a longitudinal cut across the growth pattern. As one can see, both the cancer cell density and mitotic rates have neat sharp maxima at the tumor borders in front of and opposed to the capillary vessel. Notice that the peaks for division rates are significantly narrower than those for cancer cell density, demonstrating that the proliferative fraction of the tumor comprises just a small part

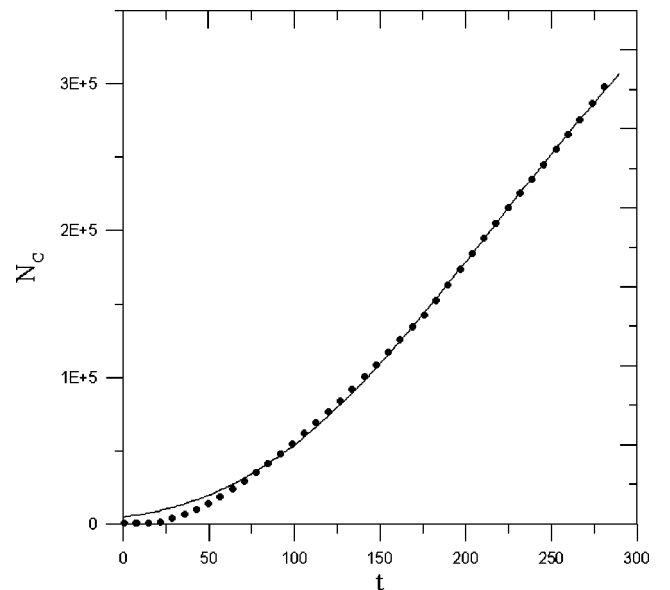


FIG. 3. Gompertz growth of cancer cell population. The model parameters were fixed at $\alpha=2/L$, $\lambda_M=10$, $\lambda_N=200$, $\theta_{\text{div}}=0.3$, $\theta_{\text{mov}}=2$, and $\theta_{\text{del}}=0.03$. The solid line corresponds to a nonlinear fitting with $r^2=0.9995$.

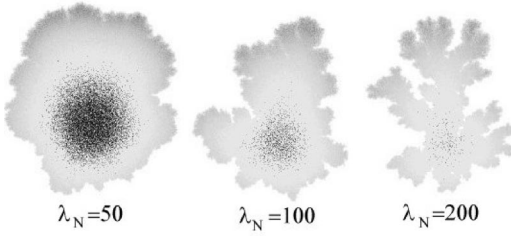


FIG. 4. Simulated growth patterns exhibiting a necrotic core (in black). The model parameters are $\alpha=2/L$, $\lambda_M=25$, $\theta_{div}=0.3$, $\theta_{mov}=\infty$ (without cell migration), and $\theta_{del}=0.03$. The fraction of necrotic cells is smaller for papillary patterns than compact ones, suggesting that the optimal growth morphology under strong nutrients limitation is fractal.

of the cancer cells localized at the tumor border.

However, in the present nutrient-limited model the disconnected patterns common in cancers of round cells [Fig. 1(e)] correspond to transient behaviors of the model for low mitotic rates and high cell migration of cancer cells. Also, the ramified morphology of a trichoblastoma seen in Fig. 6(d) could not be qualitatively reproduced by the model. A worthwhile feature of this pattern is the presence of “leaves,” the growth of each one clearly influencing the others. The simple introduction of cell motility sensitive to the nutrient gradients failed to generate stationary disconnected or ramified patterns. Therefore, in addition to the nutrient field, it appears that a chemotactic interaction among cancer cells guiding their migration must be in action. The nature of this biological interaction and the results of its simulation will be focused on in Sec. IV.

IV. GROWTH FACTORS

From the biological point of view the chemotactic response to growth factors released by cancer cells seems to be, in addition to nutrient supply, another central feature in cancer development. The reciprocal influence among cancer cells mediated by autocrine and paracrine growth factors, motility factors, etc., influence the microenvironment of each

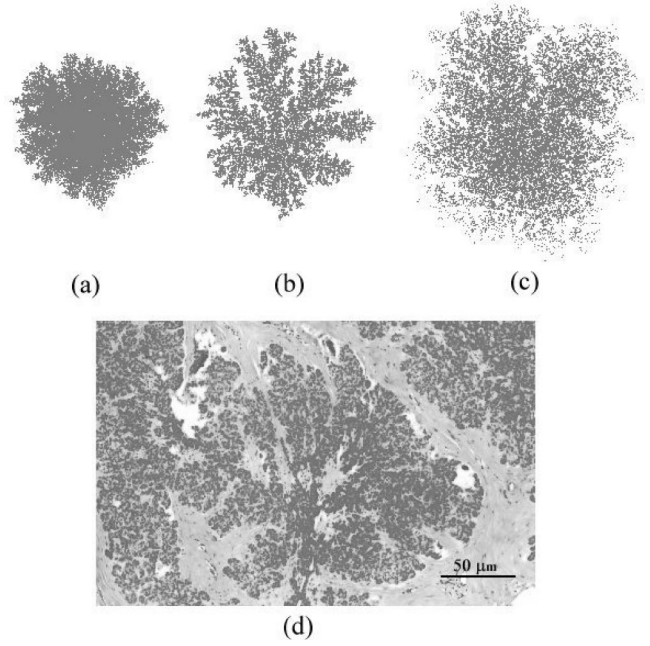


FIG. 6. Simulated patterns of the nutrient-limited cancer growth model including the influence among cancer cells mediated by growth factors. (a) compact ($k=0.1$ and $\theta_{mov}=1$), (b) ramified ($k=0.025$ and $\theta_{mov}=1$) morphologies, and (c) disconnected ($k=0.025$ and $\theta_{mov}=0.1$). The remaining parameters of the model were fixed at $\alpha=3/L$, $\theta_{div}=0.5$, $N^*=\theta_{del}=0.01$, $\lambda=5$ and $\Gamma=10$. The tissue size is 500×500 , with the initial “cancer seed” 300 sites distant from the capillary and the total number of cancer cells is 5×10^4 . For comparison, a real ramified pattern observed in trichoblastoma is shown in (d).

cancer cell and hence its division and migration. Thus, both diffusive fields (nutrients and growth factors) determine the local probabilities for cancer cells to divide, migrate, and die.

A. The model

In order to investigate the role of growth factors in a nutrient-limited growth, we simplify our model by considering a single nutrient field described by the diffusion equation,

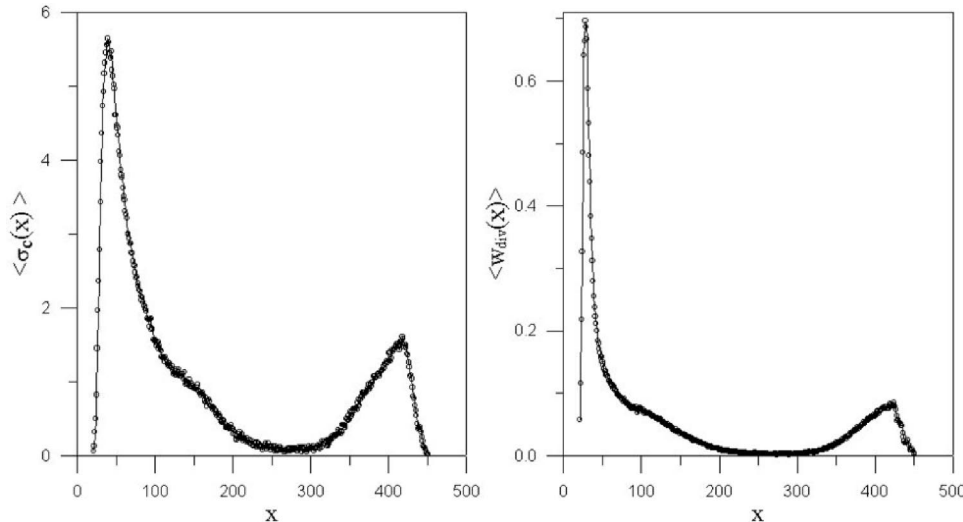


FIG. 5. (a) Density of cancer cells σ_c and (b) division rates w_{div} as a function of the distance from the capillary vessel along a tumor longitudinal cut. The model parameters were fixed at $\alpha=2/L$, $\lambda_M=25$, $\lambda_N=50$, $\theta_{div}=0.3$, $\theta_{mov}=\infty$ (without cell migration), and $\theta_{del}=0.03$. Sharp maxima at the tumor borders near and opposed to the capillary vessel at $x=0$ are evident. Therefore, the proliferative fraction of cancer cells is distributed in a thin shell on the tumor border.

$$\frac{\partial N}{\partial t} = D_N \nabla^2 N - \gamma N \sigma_n - \lambda \gamma N \sigma_c, \quad (11)$$

in which γ and $\lambda\gamma$ are the nutrient consumption rates of normal and cancer cells, respectively. The boundary conditions are the same described in Sec. II. In turn, the growth factor (GF) concentration obeys the diffusion equation

$$\frac{\partial G}{\partial t} = D_G \nabla^2 G - k^2 G + \Gamma \sigma_c N (G_M - G), \quad (12)$$

which includes the natural degradation of GFs, also imposing a characteristic length $\sim 1/k$ for GFs diffusion, and a production term increasing linearly with the local nutrient concentration up to a saturation value G_M . Therefore, we are assuming that the release of GFs involves complex metabolic processes supported by nutrient consumption. The boundary conditions satisfied by the GF concentration field is $G(\vec{x}, t) = 0$ at a large distance ($d > 2/k$) from the tumor border.

Again, the number of parameters in Eqs. (9) and (10) can be reduced by using the new dimensionless variables,

$$t' = \frac{D_N t}{\Delta^2}, \quad \vec{x}' = \frac{\vec{x}}{\Delta}, \quad N' = \frac{N}{K_0}, \quad G' = \frac{G}{G_M},$$

$$\alpha = \left(\frac{\gamma \Delta^2}{D_N} \right)^{1/2}, \quad k' = k \left(\frac{\Delta^2}{D_N} \right)^{1/2}, \quad \Gamma' = \frac{\Gamma \Delta^2}{D_N}, \quad D = \frac{D_G}{D_N}. \quad (13)$$

Using these new variables in Eqs. (9) and (10) and omitting the primes, we obtain

$$\frac{\partial N}{\partial t} = \nabla^2 N - \alpha^2 N \sigma_n - \lambda \alpha^2 N \sigma_c \quad (14)$$

and

$$\frac{\partial G}{\partial t} = D \nabla^2 G - k^2 G + \Gamma \sigma_c N (1 - G) \quad (15)$$

for the diffusion equations. The boundary condition for the nutrients on the capillary vessel becomes $N(x=0) = 1$ and a value $\Delta = 1$ is defined. In addition, in the stationary state the parameter D in Eq. (13) can be put equal to unity by rescaling the parameters k and Γ . So, the diffusion equations for the nutrients and GFs involve four parameters.

On the other hand, the cell dynamics has essentially the same rules used in Sec. II, but with different cell action probabilities. The single change introduced is that after cell division the daughter cell stands at the same site occupied by its mother. Since nutrients are essential to the large protein and DNA synthesis necessary for cell mitosis and GFs act as mitotic inductors, the proposed form of P_{div} is

$$P_{\text{div}}(\vec{x}) = 1 - \exp \left[- \left(\frac{N}{\sigma_c} - N^* \right) \frac{G^2}{\theta_{\text{div}}^2} \right]. \quad (16)$$

The parameter N^* determines the nutrient-poor level below which the cancer cells' reproduction is inhibited.

Cell migration involves large cytoskeleton reorganizations that consume energy and is facilitated by GFs, which destroy the extracellular matrix and the adhesivity structures between normal cells. Thus, P_{mov} is written as

$$P_{\text{mov}}(\vec{x}, \vec{x}') = 1 - \exp \left[\frac{N(\vec{x}) G(\vec{x}) [G(\vec{x}) - G(\vec{x}')]]}{\theta_{\text{mov}}} \right], \quad (17)$$

implying that a cell migrates in a gradient-sensitive way towards sites where the GF concentration is lower than that at its starting point.

Finally, cell death is produced by the lack of nutrients,

$$P_{\text{del}}(\vec{x}) = \exp \left[- \left(\frac{N}{\sigma_c \theta_{\text{del}}} \right)^2 \right]. \quad (18)$$

B. Results

In Fig. 6 typical compact, ramified, and disconnected simulated patterns are shown. The ramified structure shown in Fig. 6(b) should be compared with the pattern of a trichoblastoma exhibited in Fig. 6(d). In contrast to the compact fingers of the papillary patterns of the preceding section, in these ramified morphologies the tumor has fjords and tips similar to those observed in DNA patterns. We emphasize that without chemotactic signaling among cancer cells the nutrient-limited model cannot generate stationary disconnected patterns. The reason is that on average GFs drive cell migration outward, promoting the tumor expansion and, in consequence, generating disconnected patterns for high cell motility. Again, the patterns were characterized by its gyration radius R_g , total number of cancer cells N_C , and number of cells on tumor periphery S . Essentially the same results were obtained for cancer progress in time, scaling relations, and spatial structures, exhibiting a central necrotic core, an inner rim of quiescent cells and a narrow outer shell of proliferating cells.

V. CONCLUSIONS

A nutrient-limited model for the growth of avascular tumors was investigated by numerical simulation. In its original version, cell proliferation, motility, and death were locally regulated by the concentration of nutrients supplied by a distant capillary vessel. These nutrients were divided into two groups, the first associated with the usual metabolic cell needs and the second essential to the synthesis of proteins and nucleic acids involved in cell division. The nutrient concentration fields were determined by solving the diffusion equation on the square lattice modeling the primary tissue. Our simulation results show that the progress in time of the total number of cancer cells, tumor gyration radius, and number of cells on the tumor border is described by Gompertz curves. The compact and papillary or fingerlike morphologies generated obey different scaling laws for different numbers of peripheral cancer cells. For compact patterns $S \sim N_C^{1/2}$ as in the Eden model, whereas for papillary patterns the exponent in the power law increases towards unity as the nutrient consumption increases, indicating a fractal morphol-

ogy for the tumor. Since in this model the cell migration is not driven by chemotactic signals secreted by the cancer cells, cell motility contributes to round and homogenize the growth patterns. Also, the simulated tumors incorporate a spatial structure composed of a central necrotic core, an inner rim of quiescent cells and a narrow outer shell of proliferating cells, in agreement with biological data.

In order to simulate disconnected and ramified tumor patterns, typical of round cells tumors and trichoblastoma, a chemotactic interaction among cancer cells mediated by growth factors was added to the competition for nutrients. Again, similar results were obtained for cancer progress in time and scaling relations. Thus, the Gompertz law emerges as a robust feature of the nutrient-limited model of cancer growth.

Despite the encouraging results for the progress curves, scaling laws, and growth patterns morphologies, including nonspherical symmetries, the major feature of the present

paper is an attempt to connect the macroscopic diffusion equations for nutrients and/or growth factors to cell response and interactions at the microscopic scaling through an effective kinetic cellular model. Indeed, the local probabilities P_{div} , P_{mov} , and P_{del} describe in a stochastic way the dynamical processes occurring in cell populations as a response to the nutrient and growth factor diffusive fields. Finally, further studies on angiogenesis, therapy, and tumor-host interactions using variants of the present model are in progress.

ACKNOWLEDGMENTS

The authors would like to thank Dr. Lissandro Conceição from the UFV Veterinary Department for kindly providing us with the histological sections of the tumors. This work was partially supported by the Brazilian agencies CNPq and FAPEMIG.

-
- [1] D. Hanahan and R. A. Weinberg, *Cell* **100**, 57 (2000).
 - [2] W. H. Clark, *J. Cancer* **64**, 631 (1991).
 - [3] G. I. Evan and K. H. Vousden, *Nature (London)* **411**, 342 (2001).
 - [4] L. Israel, *J. Theor. Biol.* **178**, 375 (1996).
 - [5] L. A. Liotta and E. C. Kohn, *Nature (London)* **411**, 375 (2001).
 - [6] I. Golding, Y. Kozlovsky, I. Cohen, and E. Ben-Jacob, *Physica A* **260**, 510 (1998).
 - [7] Y. Kozlovsky, I. Cohen, I. Golding, and E. Ben-Jacob, *Phys. Rev. E* **59**, 7025 (1999).
 - [8] S. S. Cross, *J. Pathol.* **182**, 1 (1997).
 - [9] T. Sato, M. Matsuoka, and H. Takayasu, *Fractals* **4**, 463 (1996).
 - [10] R. L. Mendes, A. A. Santos, M. L. Martins, and M. J. Vilela, *Physica A* **298**, 471 (2001).
 - [11] G. J. Pettet, C. P. Please, M. J. Tindall, and D. L. S. McElwain, *Bull. Math. Biol.* **63**, 231 (2001).
 - [12] N. Bellomo and L. Preziosi, *Math. Comput. Modell.* **32**, 413 (2000).
 - [13] H. A. Levine, S. Pamuk, B. D. Sleeman, and M. Nilsen-Hamilton, *Bull. Math. Biol.* **63**, 801 (2001).
 - [14] E. De Angelis and L. Preziosi, *Math. Models Methods Appl. Sci.* **10**, 379 (2000).
 - [15] S. C. Ferreira Jr., M. L. Martins, and M. J. Vilela, *Physica A* **261**, 569 (1998).
 - [16] S. C. Ferreira Jr., M. L. Martins, and M. J. Vilela, *Physica A* **272**, 245 (1999).
 - [17] P. C. Nowell, *Science* **194**, 23 (1976).
 - [18] M. Scalerandi, A. Romano, G. P. Pescarmona, P. P. Delsanto, and C. A. Condat, *Phys. Rev. E* **59**, 2206 (1999).
 - [19] M. Scalerandi, G. P. Pescarmona, P. P. Delsanto, and B. Capogrosso Sansone, *Phys. Rev. E* **63**, 011901 (2000).
 - [20] A. Friedman and F. Reitich, *Math. Models Methods Appl. Sci.* **11**, 601 (2001).
 - [21] A. Brú, J. M. Pastor, I. Feraud, I. Brú, S. Melle, and C. Berenguer, *Phys. Rev. Lett.* **81**, 4008 (1998).